





OPEN

Load frequency stabilization of distinct hybrid conventional and renewable power systems incorporated with electrical vehicles and capacitive energy storage

Amil Daraz^{1,5}, Hasan Alrajhi², Abdul Basit¹, Abdul Rahman Afzal³, Ahmed N. M. Alahmadi² & Irfan Ahmed Khan⁴

Maintaining a power balance between generation and demand is generally acknowledged as being essential to maintaining a system frequency within reasonable bounds. This is especially important for linked renewable-based hybrid power systems (HPS), where disruptions are more likely to occur. This paper suggests a prominent modified “Fractional order-proportional-integral with double derivative (FOPIDD2) controller” as an innovative HPS controller in order to navigate these obstacles. The recommended control approach has been validated in power systems including wind, reheat thermal, solar, and hydro generating, as well as capacitive energy storage and electric vehicle. The improved controller’s performance is evaluated by comparing it to regular FOPID, PID, and PIDD2 controllers. Furthermore, the gains of the newly structured FOPIDD2 controller are optimized using a newly intended algorithm terms as squid game optimizer (SGO). The controller’s performance is compared to benchmarks such as the grey wolf optimizer (GWO) and jellyfish search optimization. By comparing performance characteristics such as maximum frequency undershoot/overshoot, and steady time, the SGO-FOPIDD2 controller outperforms the other techniques. The suggested SGO optimized FOPIDD2 controller was analyzed and validated for its ability to withstand the influence of power system parameter uncertainties under various loading scenarios and situations. Without any complicated design, the results show that the new controller can work steadily and regulate frequency with an appropriate controller coefficient.

Keywords Load frequency regulation, Fractional order controller, Renewable energy resources, Heuristic algorithm, Squid game optimizer, Interconnected power system

A sharp increase in demand, coupled with greater exhaustion of fossil fuels, is driving the use of unconventional resources in today’s electricity grid. The transition of an energy system with low emissions and its adoption of policies has been detailed in references^{1,2}. In this situation, a hybrid power system combined with non-conventional supplies is thought to be the cheapest option due to its energy security, on-site allocated energy supply and small-scale analysis. However, mismatches between net production and demand are common in hybrid power systems, causing frequency and power fluctuations. To evade this difficulty in the current power system modeled, automatic load frequency regulator serves an important role in preserving the equilibrium between consumption and production through system frequency management and power allocation. The

¹College of Information Science and Electronic Engineering, Zhejiang University, Hangzhou, China. ²Electrical Engineering Department, College of Engineering and Islamic Architecture, Umm Al-Qura University, Makkah 21955, Saudi Arabia. ³Department of Industrial Engineering, University of Business and Technology (UBT) University, Jeddah, Saudi Arabia. ⁴Department of Electrical Engineering, Faculty of Engineering, Universiti Malaya, Kuala Lumpur, Malaysia. ⁵MEU Research Unit, Middle East University, Amman, Jordan. ✉email: amil.daraz@zju.edu.cn; a.afzal@ubt.edu.sa

frequency variation is mostly governed by both main and auxiliary controls³. Secondary control plays a vital role in regulating frequency after significant deviations or incidents while a governor has a control procedure that allows it to modify speed and frequency in elementary control^{4,5}. As a result, secondary control is vital in regulating frequency after significant deviations or incidents⁴. Renewable energy storages (RESs) technology yields an abundance of benefits, including the reduction of greenhouse gas emissions and the improvement of sustainability of the energy system, despite their draw backs of lower inertia and intermittent behavior^{6,7}.

Literature study

Considerable support has been made by the researchers in order to tackle the frequency regulation issue in the PS. For instance, the authors has examined Load Frequency Control (LFC) in single-area systems (referenced as^{8,9}), deregulated energy grids (referenced as^{10,11}), and multi-zone systems with non-linearities (referenced as^{12–14}). To manage load frequency in power systems, numerous control mechanisms have been implemented, including robust sliding mode controllers¹⁵, model predictive control reference in¹⁶, linear-matrix inequality¹⁷, artificial intelligence-based LFC¹⁸, resilient control methodologies¹⁹, data-driven controllers²⁰, and robust virtual inertia control²¹ and fuzzy logic control (FLC) referenced as²². Historically, the PID controller has been the predominant choice for regulating the frequency of interconnected power systems owing to its straightforwardness and economical nature. However, adjusting the PID controller to account for nonlinear characteristics and system interruptions is difficult and necessitates considerable experimentation in order to ascertain the most effective PID values. There has been a surge in interest regarding the utilization of fractional order controllers for power optimization control due to recent developments in computing power. Significantly, secondary LFCs have been implemented using FOPID and its modifications in interconnected two-region power systems^{23–25}. Additionally, cascaded controller types^{26–28} have been implemented in an effort to improve frequency stability. Modern studies^{29,30} investigate a dual-controller integration strategy, with a particular focus on the PIDD2 controller framework, which was introduced in³¹ to mitigate frequency fluctuations in a two-area coupled power system. Furthermore, for frequency adaptation of the system, the literature^{32,33} suggests the integral-tilt derivative (ITD) and FOI-TD controllers; of these, the ID-T controller exhibits greater frequency efficacy than the TID controller³⁴. Fractional calculus has been extensively applied to improve upon traditional PID controllers. In numerous engineering applications, including LFC systems, FOPID and PIDD2 controllers have proven to be advantageous. In order to enhance the transient and dynamic performance of LFCs, we present an innovative FOPIDD2 controller. This controller forms a hybrid framework by integrating PIDD2 and fractional calculus.

Aforementioned research illustrates that the selection of the controller type is equally as crucial as the selection of the controller parameters. The implementation of evolutionary optimization for controller parameter optimization has resulted in a significant enhancement of the frequency stability issue. Sophisticated new techniques are implemented in order to optimize the controller parameters and surmount the intricacy of the control schemes. As an illustration, the authors implemented the following algorithms: self-tuned algorithm (STA)³⁵, Bull–Lion Optimization (BLO)³⁶, Differential Evolution based PI regulator for automatic generation control³⁷, chaos game optimization (CGO)³⁸, Krill herd algorithm for AGC of multi-region non-linear power system³⁹, improved fitness dependent algorithm based tuned modified FOPID controller employed in deregulated environment⁴⁰, modified multiverse optimizer⁴¹, and Sunflower optimization algorithm (BOA)⁴². The authors in⁴³ have been using pathfinder optimizer algorithm (PFA) to balance load power demand employing FOTID regulator. According to research⁴⁴, the I/PI/PID controller was surpassed by the TID with filter (TIDF) configured with DE. In a similar vein, the efficacy of the modified tilt integral derivative controller optimized with the water cycle algorithm (WCA) surpassed that of PID/TID controllers⁴⁵.

The present study introduces a recent and strong metaheuristic algorithm called the Squid Game Optimizer (SGO) that draws inspiration from the fundamental principles of a traditional Korean sport in order to determine the optimal parameters for the proposed FOPIDD2 controller. Assailants aim to achieve their objective during the cephalopod game, whereas teams compete to eliminate one another. It is generally executed on expansive, unrestricted areas lacking any predetermined boundaries regarding scope or dimensions. Historical records indicate that the court for this sport is typically squid-shaped and seems to be half the size of a normal basketball court. The mathematical formulation of this approach is initially constructed through the random selection of optimal candidate solutions and an initialization method. Solution candidates engage in combat with defensive players in two groups, instigating a rematch that involves arbitrary movement in the opposite direction. The position update procedure has been finalized, and the champion states of the players on opposing factions are utilized to generate the current position vectors. The estimates for these states are derived from the cost function. The performance of the presented SGO algorithm is evaluated using twenty-five (25) unrestricted mathematical assessment functions in addition to six other commonly employed metaheuristics for assessment. In addition, the capability of the proposed SGO is assessed through the utilization of sophisticated real-world challenges on the most recent CEC-2020⁴⁶. The SGO exhibits exceptional performance in addressing these thought-provoking optimization issues.

Furthermore, an extensive review of the relevant literature leads to the fundamental conclusion that LFC methods, including FLC, model predictive control (MPC) and H-infinite approaches achieve the desired performance despite a protracted setup process and numerous design flaws. Furthermore, traditional PD, PI, and PID controllers encounter difficulties when confronted with system uncertainty. In a number of earlier works, the influence of boundary fluctuations and system nonlinearities on robustness evaluations was inadequately investigated. The majority of prior assessments failed to account for the substantial incorporation of renewable energy sources, despite the inclusion of nonlinear system uncertainties and immediate fluctuations in demand, without modifying system parameters.

Contribution of the paper

FOPIDD2 controller is presented in this study with the objective of improving the frequency stability of the system while accounting for disturbances caused by renewable energy sources. In accordance with the tenets of the SGO, the parameters of the FOPIDD2 controller that has been proposed have been adjusted to guarantee frequency stability and system performance under atypical circumstances. The principal contributions of this paper, relative to previous investigations on analogous subjects, encompass:

- Incorporating an efficient FOPIDD2 controller into dual zone coupled power systems that incorporate Capacitive Energy Storage (CES), Renewable Energy Sources (RES), and Electric Vehicles (EVs) in order to enhance frequency stability.
- Introducing a strong robust algorithm, the Squid Game Optimizer (SGO), to fine-tune the parameters of the presented FOPIDD2 controller.
- Validating the superiority of the proposed FOPIDD2 controller over existing PID/PID/ FOPID controllers.
- Demonstrating the effectiveness of the Squid Game Optimizer in comparison to other contemporary algorithms, such as the Grey Wolf Optimizer (GWO) and Jellyfish Swarm Optimization (JSO).
- Assessing the resilience of the suggested controller in the presence of significant fluctuations in all system parameters, and random load disturbances.

Investigation of hybrid power systems including non-linearities

This section presents a mathematical representation of a combined dual-area power system (PS), which includes renewable energy resources, electric vehicles, capacitor energy storage, and conventional power sources as shown in Fig. 1. The distribution of renewable energy sources (RESs) occurs in distinct zones, where zone 1 comprises solar power and zone 2 comprises wind power. Zone 1 is comprised of a thermal resource, whereas Zone 2 is a hydroelectric structure. It is presumed that the distribution of electric vehicles between the two regions is equivalent. The components used to build the PS system are sourced from^{7,47} and implemented in the Simulink/ Matlab environment; additional information is available in Appendix A. The performance of the suggested controllers is significantly influenced by the nonlinearities demonstrated by the components of the system; therefore, it is vital to take these into account during the design and testing stages. The physical constraints of power plants are accounted for by the system under investigation, which includes the governor dead band (GDB) and generation rate constraint (GRC) of thermal units. Both the ascending and decreasing rates have a 10% pu/min (0.0017 pu.MW/s) GRC^{28,33}. In addition, the hydropower plant is subject to GRC constraints, which stipulate that the rates of increase and decrease are 270 percent pu/min (0.045 pu.MW/s) and 360 percent pu/

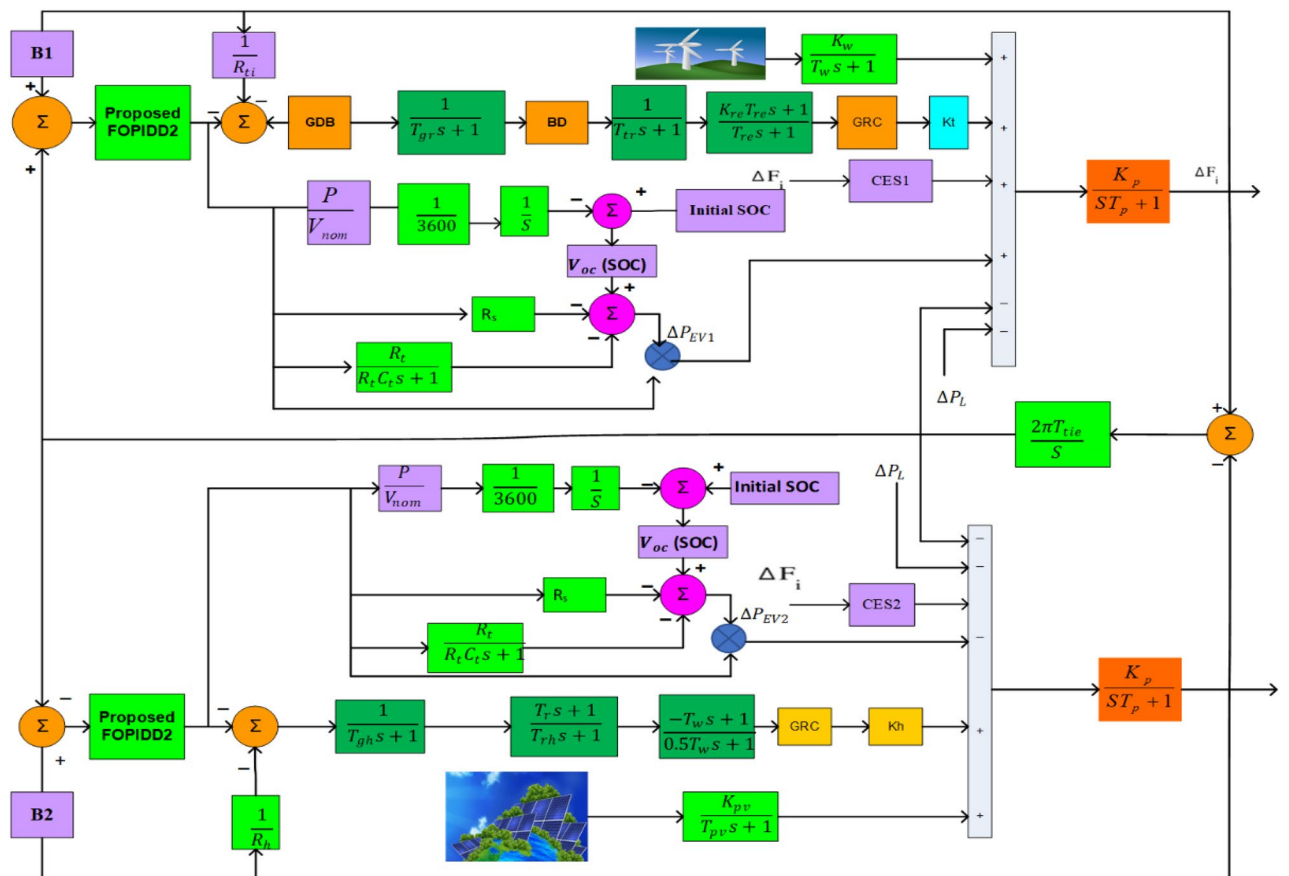


Figure 1. Schematic modelling of proposed HPS.

min (0.06 pu.MW/s), respectively. Upon linearization, the GDB can be represented by the speed change and its rate of change, resulting in a Fourier series transfer function model that incorporates a 0.5 percent backlash^{28,33}. The formulation of this model is as follows:

$$\text{GDB} = \frac{N_1 + SN_2}{T_{sg}S + 1} \quad (1)$$

$$\text{Where } N_1 = 0.8 \text{ and, } N_2 = \frac{-0.2}{\pi} \quad (2)$$

Modelling of conventional power systems

Traditional power generation systems consisted of reheat thermal (incorporating a governor-turbine-reheater sub model) and hydropower generation (incorporating a penstock-droop compensation sub model). The subsequent equations illustrate the mathematical representations for reheating thermal systems and their corresponding sub-models, which consist of a governor, turbine, and re-heater^{33,48}.

$$G_G(s) = \frac{1}{(1 + T_{gr}s)} \quad (3)$$

$$G_T(s) = \frac{1}{(1 + T_{tr}s)} \quad (4)$$

$$G_R(s) = \frac{1 + T_{re}K_{re}s}{(1 + T_{re}s)} \quad (5)$$

$$G_{RT}(s) = \frac{1 + T_{re}K_{re}s}{(1 + T_{gr}s)(1 + T_{re}s)(1 + T_{tr}s)} \quad (6)$$

The subsequent sub-models for hydroelectric power, including droop compensation, governor, and penstock, are mathematically represented by the equations listed below⁴⁸.

$$G_{HG}(s) = \frac{1}{(1 + T_h s)} \quad (7)$$

$$G_{HT}(s) = \frac{(1 + T_{rs}s)}{(1 + T_{rh}s)} \quad (8)$$

$$G_{HD}(s) = \frac{(1 - T_w s)}{(1 + 0.5T_w s)} \quad (9)$$

$$G_H(s) = \frac{(1 - T_w s)(1 + T_{rs}s)}{(1 + T_h s)(1 + 0.5T_w s)(1 + T_{rh}s)} \quad (10)$$

Modelling of capacitive energy storage (CES)

Capacitive energy storage (CES) devices are increasingly being incorporated into contemporary power systems for their notable power output and ability to rapidly charge and discharge⁴⁹. An advantage of CES is its capacity to generate an ample amount of electricity in a timely manner in response to increased demand. It is economical, straightforward to operate, and has an extended operational lifespan without sacrificing efficiency. The principal energy storage element within the CES system is a supercapacitor which stores energy in the form of static charge using capacitor plates⁵⁰. CES returns energy that has been stored to the grid during times of high demand. Equation (18) illustrates the variation in the incremental power of CES⁵¹.

$$\Delta P_{CES} = \left[\frac{K_{CES}}{1 + sT_{CES}} \right] \left[\frac{1 + sT_1}{1 + sT_2} \right] \left[\frac{1 + sT_3}{1 + sT_4} \right] \Delta F \quad (11)$$

The time constants of the two-stage phase compensation blocks are denoted as T1–T4.

Modelling of electrical vehicles (EVs)

The recent modification of EVs for regular vehicles in power grids allows for the use of their built-in batteries. Thus, EV batteries with consistent batteries can be regulated to increase frequency adaptability in remote microgrids. EVs also eliminate the need for additional energy storage units in these systems. As a result, EVs can lower system costs and improve the functioning of distant microgrids (MGs). To execute several potential activities, it is necessary to be able to simulate the dynamics of EV energy storage in order to optimize power

system sizing, supervision, and control. To express EV functionality in LFC^{52,53}, an equivalent Thevenin-based EV representation is used and connected to the dual region power system, as shown in Fig. 2. In this concept, V_{oc} represents the voltage of an open-circuit battery. The voltage of the EVs is ultimately determined by the state of charge (SOC) and voltage of the batteries as shown in below equation⁵⁴.

$$V_{oc}(SOC) = S \frac{RT}{F} \ln \left(\frac{SOC}{C_{nom} - SOC} \right) + V_{nom} \tag{12}$$

where C_{nom} and V_{nom} are the nominal contents and batteries voltage powering the EV. The sensitivity parameter is denoted by S , the gas constant is denoted by R , the Faraday constant is denoted by F , and the temperature constant is denoted by T .

Solar and wind generation modelling

PV service functionality is established by solar radiation and ambient temperature. PV plants’ power output varies with the quantity of sunlight they get. Power electronics-based transfer gadgets are now widely used in PV systems to keep maximum power constant. Injecting the waveforms of high-power-quality currents, they also perform the grid amalgamation function. The execution of power system stability suffers because of fluctuations in output power. The following expression is a model for the power output of solar power plants^{55,56}.

$$P = \eta \varphi_{solar} S [1 - 0.005(T_a + 25)] \tag{13}$$

where φ_{solar} stands for solar insolation, η for the PV panel’s conversion efficiency, T_a for the ambient temperature, and S for the PV area. In this study, a realistic PV output power has been built to imitate PV inconsistent features based on the design from reference⁵⁷.

$$G_{PV}(s) = \frac{K_{PV}}{T_{PV}s + 1} \tag{14}$$

where T_{PV} is the time constant in the PV model and K_{PV} is the gain constant.

On the other side, the main factor causing the sporadic characteristics of wind farms is the mechanical wind turbine (WT) power output’s wind speed associated power fluctuating using the below expression^{57,58}.

$$P_{wind} = 1/2 \rho A_r C_p V_{\omega}^3 \tag{15}$$

where C_p is the power coefficient, A_r is the swept area, ρ is the air density, and V_{ω} is the wind speed. In this study, a realistic wind output power is created based on the model from^{57,58} to replicate wind erratic features. A model representation of $G_w(s)$ is shown below⁵⁸.

$$G_w(s) = \frac{K_T}{T_T s + 1} \tag{16}$$

where the wind model’s time constant is denoted by T_T , and its gain constant is denoted by K_T .

Squid game optimizer (SGO)

The Squid Game Optimizer (SGO) method, which draws inspiration from the fundamental principles of a traditional Korean game⁴⁶, is presented as a novel metaheuristic algorithm. In the squid game, teams compete to eliminate one another on open fields with no predetermined size restrictions, while attackers strive to attain their objective. The game court, which has a historical cephalopod shape and is approximately half the size of

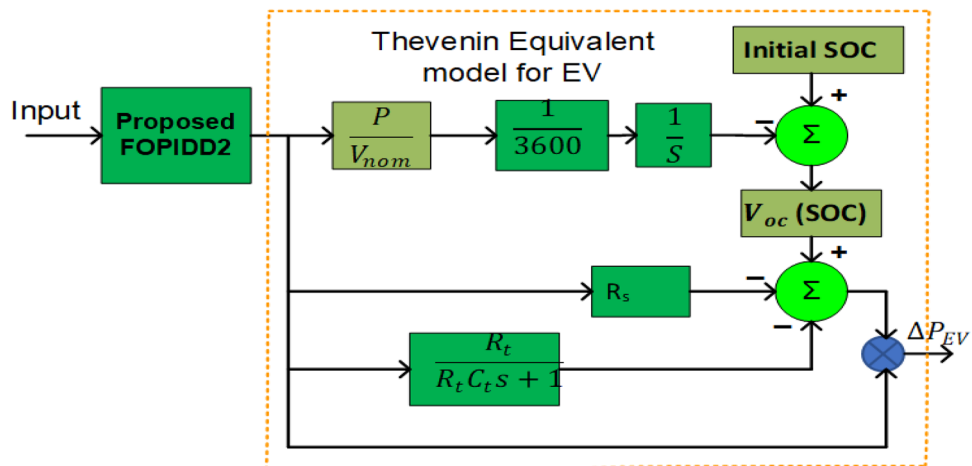


Figure 2. Modeling of EVs for the proposed system.

a typical basketball court, functions as the foundation for the mathematical formulation of the algorithm. The algorithm begins by generating its model through the random selection of optimal candidate solutions and an initialization method. The candidates then alternate between two groups of defensive players during a simulated battle. A cost function is utilized to ascertain the champion states of players on opposing factions during the position update procedure. In order to evaluate the performance of the algorithm, twenty-five unrestricted mathematical evaluation functions are applied in conjunction with six prevalent metaheuristics. Furthermore, the efficacy of the SGO is evaluated using real-world scenarios sourced from the most recent CEC (CEC 2020), which unveils remarkable outcomes in addressing intricate optimization issues. The SGO algorithm is comprised of the subsequent stages:

Mathematical formulation

The mathematical description of the SGO as a metaheuristic method employing the squid game strategy is elaborated in this section. In the first phase, the initialization technique is implemented as follows, considering the seek space to be a distinct region of the field and the potential candidates (X_i) to be players⁴⁶:

$$X = \begin{bmatrix} X_1 \\ X_2 \\ \vdots \\ X_i \\ \vdots \\ X_n \end{bmatrix} = \begin{bmatrix} x_1^1 x_1^2 \dots x_1^j \dots x_1^d \\ x_2^1 x_2^2 \dots x_2^j \dots x_2^d \\ \dots \vdots \vdots \\ x_i^1 x_i^2 \dots x_i^j \dots x_i^d \\ \dots \vdots \vdots \\ x_n^1 x_n^2 \dots x_n^j \dots x_n^d \end{bmatrix}, \begin{cases} j = 1, 2, \dots, d \\ i = 1, 2, \dots, n \end{cases} \tag{17}$$

$$x_i^j = x_{i,\min}^j + (x_{i,\max}^j - x_{i,\min}^j) \cdot rand, \begin{cases} i = 1, 2, \dots, n \\ j = 1, 2, \dots, d \end{cases} \tag{18}$$

where n denotes the overall count of participants in the search space, d signifies the magnitude of the problem being examined, and the j th decision variable or identifies the starting position of the i th candidate. The upper and lower limits of the j th variable are denoted by $x_{i,\max}^j$ and $x_{i,\min}^j$ respectively. A random number denoted as “rand” is distributed in an even manner from 0 to 1.

$$X^{off} = \begin{bmatrix} X_1^{off} \\ X_2^{off} \\ \vdots \\ X_i^{off} \\ \vdots \\ X_m^{off} \end{bmatrix} = \begin{bmatrix} x_1^1 x_1^2 \dots x_1^j \dots x_1^d \\ x_2^1 x_2^2 \dots x_2^j \dots x_2^d \\ \dots \vdots \vdots \\ x_i^1 x_i^2 \dots x_i^j \dots x_i^d \\ \dots \vdots \vdots \\ x_m^1 x_m^2 \dots x_m^j \dots x_m^d \end{bmatrix}, \begin{cases} i = 1, 2, \dots, m \\ j = 1, 2, \dots, d \end{cases} \tag{19}$$

$$X^{Def} = \begin{bmatrix} X_1^{Def} \\ X_2^{Def} \\ \vdots \\ X_i^{Def} \\ \vdots \\ X_m^{Def} \end{bmatrix} = \begin{bmatrix} x_1^1 x_1^2 \dots x_1^j \dots x_1^d \\ x_2^1 x_2^2 \dots x_2^j \dots x_2^d \\ \dots \vdots \vdots \\ x_i^1 x_i^2 \dots x_i^j \dots x_i^d \\ \dots \vdots \vdots \\ x_m^1 x_m^2 \dots x_m^j \dots x_m^d \end{bmatrix}, \begin{cases} i = 1, 2, \dots, m \\ j = 1, 2, \dots, d \end{cases} \tag{20}$$

where m represents the whole participants in every group of games; The k th player on defense is X_i^{Def} and the i th player on offence is X_i^{off} . At the beginning of the game, one offensive player fights with the defensive players. It is important to note that while defensive players are allowed to utilize both feet, attacking players are only allowed to move and fight with one foot. The mathematical representation of these elements is as follows⁴⁶:

$$DG = \frac{\sum_{i=1}^m X_i^{Def}}{m}, i = 1, 2, \dots, m \tag{21}$$

$$X_i^{offNew1} = \frac{X_i^{off} + r_1 \times DG - r_2 \times X_{r3}^{Def}}{2}, i = 1, 2, \dots, m \tag{22}$$

The offensive players’ capabilities are represented by r_1 and r_2 , which are random values between 0 and 1. The defensive group is represented by (DG), and the i th offensive player’s future position on the ground is indicated

by $X_{r3}^{Def} \in [1 \text{ to } m]$. Each player's fitness function is assessed following a match between the i th offensive player and a particular defensive player. The winner is decided by the players' contest result. Declared the winner, the offensive player becomes a member of the winning offensive group (SOG). In order to achieve this, if the offensive player's winning status exceeds the defensive player's, the attacking player may use both feet. These aspects can be expressed mathematically as follows⁴⁶:

$$X^{Scaff} = \begin{bmatrix} X_1^{Scaff} \\ X_2^{Scaff} \\ \vdots \\ X_i^{Scaff} \\ \vdots \\ X_o^{Scaff} \end{bmatrix} = \begin{bmatrix} x_1^1 x_1^2 \dots x_1^j \dots x_1^d \\ x_2^1 x_2^2 \dots x_2^j \dots x_2^d \\ \dots \dots \vdots \\ x_i^1 x_i^2 \dots x_i^j \dots x_i^d \\ \dots \dots \vdots \\ x_o^1 x_o^2 \dots x_o^j \dots x_o^d \end{bmatrix}, \begin{cases} i = 1, 2, \dots, o \\ j = 1, 2, \dots, d \end{cases} \tag{23}$$

$$SOG = \frac{\sum_{i=1}^o X_i^{Scaff}}{o}, i = 1, 2, \dots, o \tag{24}$$

$$X_i^{offNew2} = X_i^{offNew1} + r_1 \times SOG - r_2 \times BS_i, BS_i = 1, 2, \dots, m \tag{25}$$

If defensive players' winning states exceed those of offensive players, the defensive players are declared game winners and invited to join the successful defense group. These defensive players in the group are expected to oversee guarding the bridge, a key feature of the playground. The successful defensive players navigate among the attacking players in the crowd in preparation for a new battle. The following is a mathematical representation of these constituents⁴⁶:

$$SDG = \begin{bmatrix} X_1^{Scaff} \\ X_2^{Scaff} \\ \vdots \\ X_i^{Scaff} \\ \vdots \\ X_p^{Scaff} \end{bmatrix} = \begin{bmatrix} x_1^1 x_1^2 \dots x_1^j \dots x_1^d \\ x_2^1 x_2^2 \dots x_2^j \dots x_2^d \\ \dots \dots \vdots \\ x_i^1 x_i^2 \dots x_i^j \dots x_i^d \\ \dots \dots \vdots \\ x_p^1 x_p^2 \dots x_p^j \dots x_p^d \end{bmatrix}, \begin{cases} i = 1, 2, \dots, p \\ j = 1, 2, \dots, d \end{cases} \tag{26}$$

$$OG = \frac{\sum_{i=1}^m X_i^{off}}{m}, i = 1, 2, \dots, m \tag{27}$$

$$X_i^{DefNew1} = \frac{X_i^{Def} + r_1 \times OG - r_2 \times X_{r3}^{off}}{2}, i = 1, 2, \dots, m \tag{28}$$

An additional step is added to the process as the assaulting players attempt to cross the bridge guarded by the defending units in SDG with the goal of strategically adjusting the exploitation and exploration stages of the predicted algorithm. As a result, all offensive players are authorized to engage in a position-updating operation that directs them towards the most promising candidate solution found thus far as well as a particular defending player in SDG. Below is a mathematical representation of these constituents⁴⁶:

$$X_i^{offNew1} = \frac{X_i^{Scaff} + r_1 \times BS - r_2 \times X_k^{ScDef}}{2}, \begin{cases} i = 1, 2, \dots, o \\ k = 1, 2, \dots, p \end{cases} \tag{29}$$

The best candidate for a solution is represented by BS in SOG and SDG, whereas p and o the total number that represent successful offensive and defensive players, respectively. Figure 3 shows the flowchart for the recommended SGO approach.

Controller design and formulation of fitness function

The fundamental goal of redesigning the FOPIDD2 is to improve and regulate the frequency response of a diversified power system dealing with abrupt load changes and fluctuations in renewable energy sources. This controller is suggested for both regions to reduce frequency fluctuations and associated tie-line power imbalances produced by diverse load disturbances and renewable energy variations. Traditional PID controllers, which are widely used in industries due to their simplicity and efficacy, provide the foundation of the PIDD2 structure, which adds a second-order derivative gain, comparable to the normal PID design⁵⁹. Although the FOPIDD2

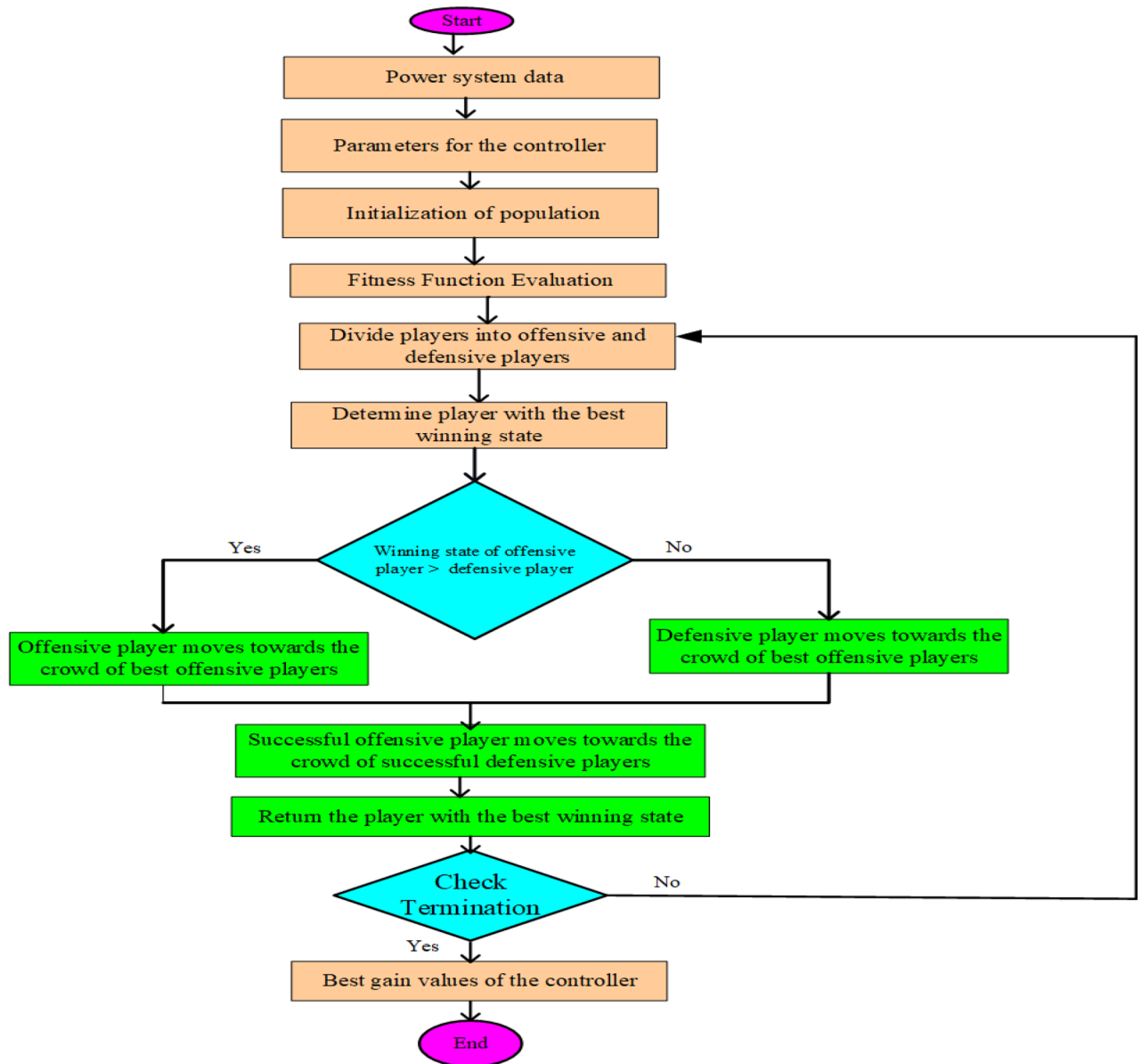


Figure 3. Flow diagram of suggested squid game optimizer.

controller has not received much attention, previous research has shown that both FOPID and PIDD2 controllers outperform typical PID controllers in terms of performance. Figure 4 shows the FOPIDD2 controller’s block diagram, which was constructed by combining the PIDD2 controller and fractional calculus. The FOPIDD2 controller, as opposed to the PIDD2 controller, incorporates the second derivative portion as a fractional order derivative^{60,61}. The transfer function of the FOPIDD2 is described in Eq. (30) and the relationship between the system’s control input (U) and the error signal (E) is described in Eq. (31).

$$FOPIDD2 = \frac{Y(s)}{R(s)} = K_p + \frac{K_i}{s^\lambda} + K_d \left[\frac{N_d s^\mu}{s^\mu + N_d} \right] + K_d \left[\frac{N_d s^\mu}{s^\mu + N_d} \right] \cdot K_{dd} \left[\frac{N_{dd} s^\mu}{s^\mu + N_{dd}} \right] \quad (30)$$

$$U(s) = E(s) \left\{ K_p + \frac{K_i}{s^\lambda} + K_d \left[\frac{N_d s^\mu}{s^\mu + N_d} \right] + K_d \left[\frac{N_d s^\mu}{s^\mu + N_d} \right] \cdot K_{dd} \left[\frac{N_{dd} s^\mu}{s^\mu + N_{dd}} \right] \right\} \quad (31)$$

where (N_d, N_{dd}) signified the filter terms, (λ, μ) are the integral-differentiator operators, and (K_d, K_p, K_i) signifies the derivative, proportional and integral knobs of the FOPIDD2 controller. The recommended gains for the FOPIDD2 controller were established by minimizing the cost function through the squid game optimizer. The adoption of an ITSE-based cost function^{33,40,48} leads to a reduction in settling time and rapid attenuation of high oscillations.

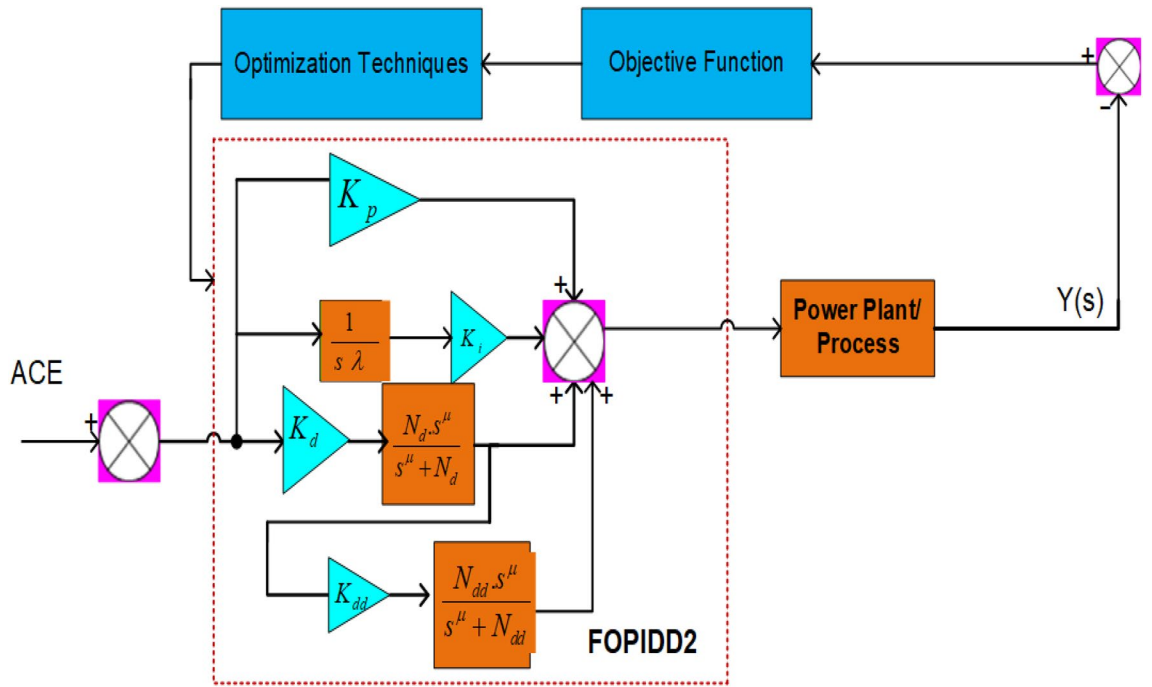


Figure 4. Structure of suggested FOPIDD².

$$ITSE = J = \int_0^t [\Delta F_1^2 + \Delta F_2^2 + \Delta P_{tie}^2] dt \tag{32}$$

$$ITAE = J = \int_0^t [|\Delta F_1| + |\Delta F_2| + |\Delta P_{tie}|] dt \tag{33}$$

$$ISE = J = \int_0^t [\Delta F_1^2 + \Delta F_2^2 + \Delta P_{tie}^2] dt \tag{34}$$

FOPIDD2 controller gains are subject to the following restrictions.

$$\begin{aligned} K_p^{Min} &\leq K_p \leq K_p^{Max}; K_d^{Min} \leq K_d \leq K_d^{Max}; \\ K_{dd}^{Min} &\leq K_{dd} \leq K_{dd}^{Max}; K_i^{Min} \leq K_i \leq K_i^{Max}; \\ N_{dd}^{Min} &\leq N_{dd} \leq N_{dd}^{Max}, N_d^{Min} \leq N_d \leq N_d^{Max}, \lambda^{Min} \leq \lambda \leq \lambda^{Max}; \\ \mu^{Min} &\leq \mu \leq \mu^{Max} \end{aligned} \tag{35}$$

Results, implementation and discussion

In this portion, the efficacy of the proposed approach is tested in a distinct hybrid power source, along with electric vehicles and capacitor energy storage. The controller knobs are optimized employing the Squid Game Optimizer (SGO) in MATLAB programming and integrated with the Simulink tool for the unified power system. The optimal values for different control algorithms have been depicted in Table 1 after 30 iterations of optimization procedures using data from Appendix B. The proposed FOPIDD2 controller, which employs the SGO approach in conjunction with the EV system, is compared to other controllers such as FOPID, PID, and PID2. The outcomes of the scrutinized multi-area Integrated Power System (IPS) are thoroughly evaluated in the following case studies.

Case-1 (analyses of controller performance)

The effectiveness of the FOPIDD2 was assessed by comparing it with several other controllers including FOPID, PID, and I-TD⁴⁵ in this scenario. The response of each controller was evaluated based on tie line power (ΔP_{tie}), area-2 (ΔF_2), and area-1 (ΔF_1), as depicted in Fig. 5a-c. Table 2 presents a comprehensive performance

Approach	K_p	K_i	K_d	K_{dd}	N_d	N_{dd}	μ	λ
SGO	3.456	1.900	1.110	2.657	6.090	5.780	0.157	0.234
JSO	5.101	2.546	2.079	8.456	8.567	4.781	0.056	0.767
GWO	1.120	2.109	1.989	3.345	3.300	4.890	0.045	0.458
FOPIDD2	4.789	3.456	3.671	9.675	8.220	7.412	0.052	0.086
FOPID	5.124	3.445	2.089	–	–	–	0.123	0.009
PIDD2	8.124	9.112	3.974	4.897	3.678	1.098	–	–
PID	4.009	1.223	7.009	–	–	–	–	–

Table 1. Optimal coefficient values for the suggested approach.

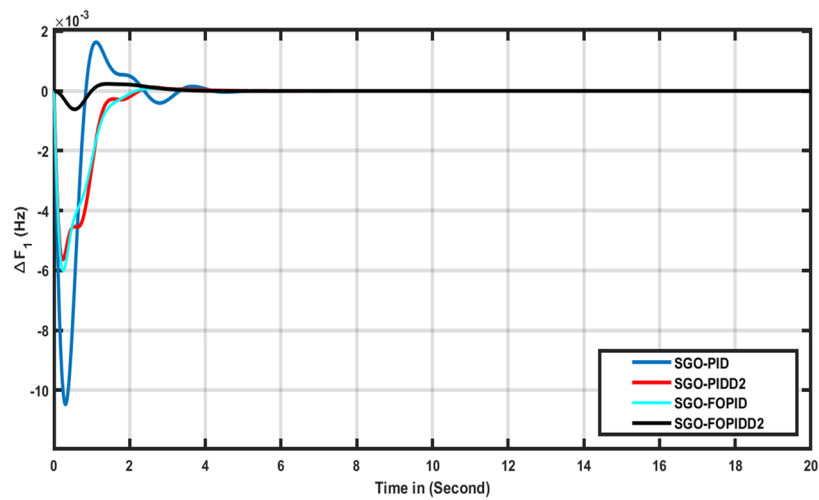
analysis of various controllers with respect to transient metrics such as Osh (Overshoot), Ush (Undershoot), and Ts (time settling) for ($\Delta F2$), (ΔP_{tie}), and ($\Delta F1$). The FOPIDD2 control strategy demonstrated faster settling times compared to PID, PIDD2, I-TD⁴⁵, and FOPID controller in regions 1, 2, and the associated tie-line. In comparison to the PID controller, the FOPIDD2 approaches reduced overshoot for ($\Delta F1$), ($\Delta F2$), and (ΔP_{tie}) by 71.66%, 87.98%, and 43.21%, respectively. Furthermore, our proposed approach enhanced the settling time by 21.66%, 19.12%, and 22.09% compared to PID controller. The FOPIDD2 controllers also improved Ts by 19.78%, 12.87%, and 26.09% when compared to the PIDD2 controller, while significantly reducing maximum Osh by 78.98%, and 67.34% for area-2 and tie line, at the cost of decreasing overshoot for area-1 and undershoot by 81.12%, 49.77%, and 08.65% for ($\Delta F1$), ($\Delta F2$), and (ΔP_{tie}). Comparing the FOPIDD2 algorithm to the I-TD⁴⁵ controller, Ts improved by 56.23% for (ΔP_{tie}), 61.34% for ($\Delta F2$), and 49.11% for ($\Delta F1$).

Case-2 (analyses of algorithm performance)

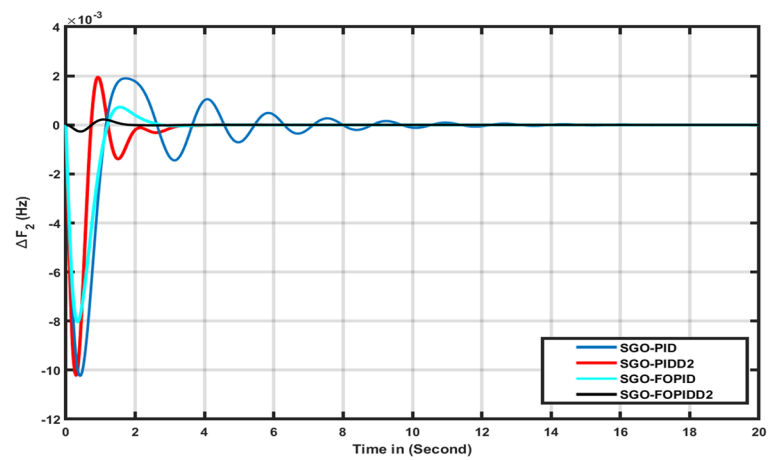
This study compared the efficacy of the squid game optimizer (SGO) with various modern algorithms including the jellyfish swarm optimization (JSO), Grey wolf optimizer (GWO), Water Cycle Algorithm (WCA)⁴⁵ and Path Finder Algorithm (PFA)⁴³. The response of each algorithm was evaluated based on tie line (ΔP_{tie}), area-2 ($\Delta F2$), and area-1 ($\Delta F1$), as depicted in Fig. 6a-c. Table 3 presents a comprehensive performance analysis of various algorithms with respect to transient metrics such as O_{sh} , U_{sh} , and T_s for (ΔP_{tie}), ($\Delta F1$), and ($\Delta F2$). From Table 3 and Fig. 7a-c it can be observed that SGO: FOPIDD2 have better settling times as compared to JSO, GWO, WCA⁴⁵, and FPA metaheuristic algorithms in regions 1, 2, and the associated tie-line. In comparison to the JSO algorithm, the SGO approaches reduced overshoot for (ΔP_{tie}), ($\Delta F1$), and ($\Delta F2$) by 27.20%, 35.11%, and 23.21%, respectively. Furthermore, our proposed approach enhanced the settling time by 34.11%, 13.43%, and 29.88% compared to grey wolf optimizer algorithms. The SGO algorithms also improved Ts by 13.98%, 47.67%, and 54.54% when compared to the jellyfish search algorithm, while significantly reducing maximum Osh by 87.09%, 81.12%, and 76.78%, and undershoot by 81.19%, 66.54%, and 93.76% for (ΔP_{tie}), ($\Delta F1$), and ($\Delta F2$). Our proposed SGO: FOPIDD2 algorithm also performed very well as compared to WCA: I-TD⁴⁵ and FPA: FOTID⁴³ approaches in respect of enhanced settling time, minimum overshoot and undershoot to the WCA: ITD optimizer algorithm for (ΔP_{tie}), area-2 ($\Delta F2$), and area-1 ($\Delta F1$).

Case-3 (Analysis of electrical vehicles and capacitive energy storage)

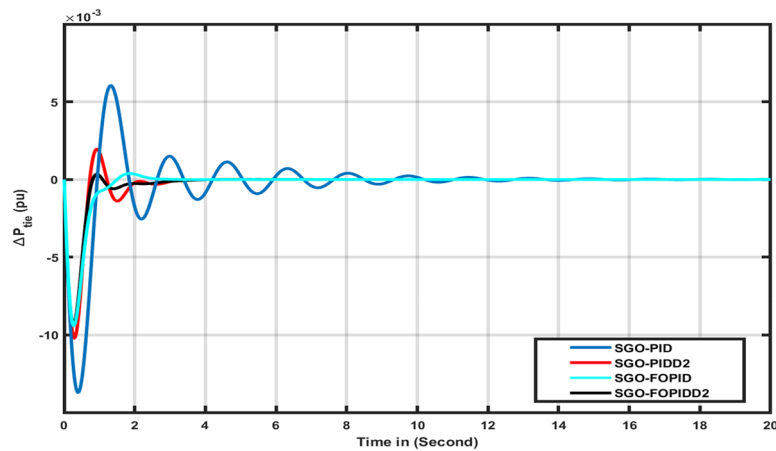
Scenario 3 assesses the outcomes of integrating Capacitor Energy Storage (CES) and Electric Vehicles (EVs) into an existing hybrid energy system. The effectiveness of the system is measured using the Squid Game Optimizer (SGO)-based FOPIDD2 controller, both with and without the effects of EVs and CES. Results for tie line (ΔP_{tie}), area-2 ($\Delta F2$), and area-1 ($\Delta F1$) are depicted in Fig. 7a-c and summarized in Table 4. The Figures illustrate that our proposed SGO-FOPIDD2, incorporating CES and EVs, outperforms in terms of reduced oscillation, undershoot, and overshoot for area-1 ($T_s = 2.88$, $O_{sh} = 0.002347$, $U_{sh} = -0.0006158$), Area-2 ($T_s = 2.60$, $O_{sh} = 0.00072454$, $U_{sh} = -0.0008038$), and tie-line ($T_s = 2.51$, $O_{sh} = 0.000120$, $U_{sh} = -0.0056199$) compared to the SGO-FOPIDD2 without CES and EV effects for Area1 ($T_s = 4.00$, $O_{sh} = 0.0024142$, $U_{sh} = -0.008772$), Tie-line ($T_s = 3.65$, $O_{sh} = 0.0019389$, $U_{sh} = -0.0102192$) and Area-2 ($T_s = 4.33$, $O_{sh} = 0.0024140$, $U_{sh} = -0.008771$). Fig. 7a-c indicates that the system's response to EVs and CES unit effects yields better outcomes in terms of Osh,



(a)



(b)



(c)

Figure 5. Transient response of HPS with various algorithm techniques in: (a) ΔF_1 (b) ΔF_2 , (c) ΔP_{tie} .

Transient parameters	Variation in areas	I-TD ⁴⁵	PID	FOPID	PID2	FOPID
Time settling	$\Delta F1$	12.27	4.01	2.83	3.29	2.22
	$\Delta F2$	29.46	11.93	2.64	3.23	1.52
	ΔP_{tie}	30.50	12.11	3.83	3.66	2.81
Overshoot	$\Delta F1$	0.00280	0.001632	0.0001233	0.0000768	0.00023470
	$\Delta F2$	0.00110	0.001890	0.0007254	0.0019490	0.0002201
	ΔP_{tie}	0.0007	0.006044	0.0017100	0.0019490	0.0003508
Undershoot	$\Delta F1$	-0.0109	-0.010480	-0.006548	-0.006016	-0.0006158
	$\Delta F2$	-0.0035	-0.010240	-0.008038	-0.010220	-0.0002686
	ΔP_{tie}	-0.0022	-0.013700	-0.010490	-0.010220	-0.009405

Table 2. Comparison performance of several controllers for case 1.

T_s , and U_{sh} for ($\Delta F1$), ($\Delta F2$), and (ΔP_{tie}) compared to the system's response without EVs and CES unit effects. Table 4 further underscores the remarkable results achieved by combining our proposed technique with EVs and CES.

Case-4 (Sensitivity analysis/robustness)

A sensitivity analysis was performed to evaluate the robustness of the optimized FOPIDD2 controller recommended by the Squid Game Optimizer (SGO). The system's stability may be compromised if the suggested control mechanism fails to adequately adjust to variations in system parameters. In order to assess the stability of the proposed controller, different metrics for parameters such as T_{gr} , T_{gh} , and K_w have been modified by about $\pm 50\%$ and compared to their original parameter responses. Figures 8, 9 illustrate the reliability of the proposed controller by varying the system parameters of the hybrid power systems. The parameters in Table 5, nearly match their nominal values, indicating that the proposed SGO-FOPIDD2 controller consistently performs well within a range of around $\pm 50\%$ of the system's characteristics. Moreover, the optimal values of the suggested controller avoid the necessity of resetting when implemented with the real values at the specified value throughout a broad spectrum of parameters. Figure 10 represents the random load variation for the hybrid

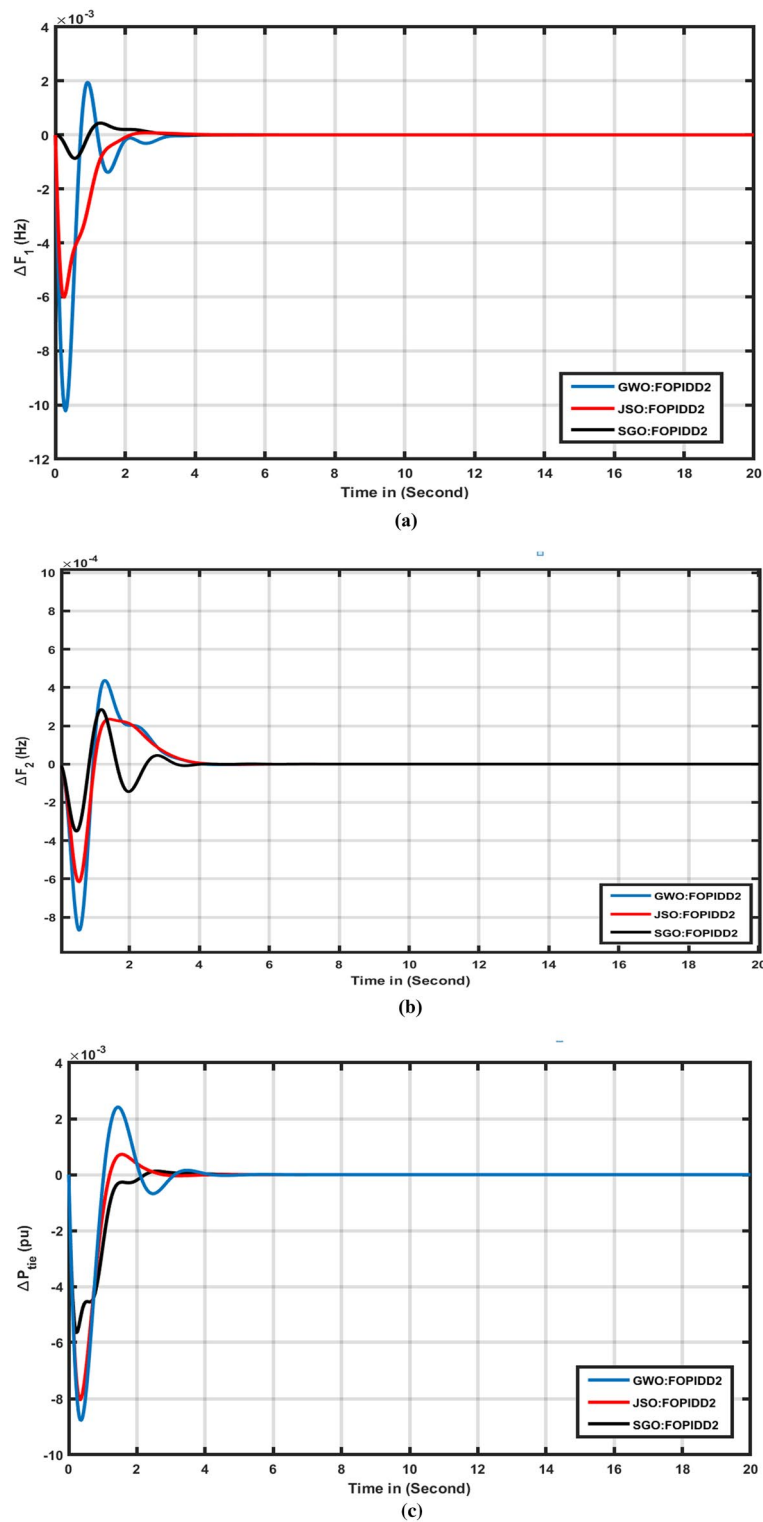


Figure 6. Transient response of HPS with various algorithm techniques in: (a) ΔF_1 (b) ΔF_2 , (c) ΔP_{tie} .

Transient parameters	Variation in areas	JSO: FOPIDD2	GWO: FOPIDD2	SGO: FOPIDD2	WCA: I-TD ⁴⁵	PFA: FOTID ⁴³
Time settling (Ts)	ΔF_1	3.66	3.80	2.86	12.27	25.5
	ΔF_2	4.09	4.85	3.93	29.46	23.2
	ΔP_{tie}	3.71	3.83	3.66	30.50	18.77
Overshoot (O_{sh})	ΔF_1	0.00007	0.00194	0.00043	0.00280	0.00680
	ΔF_2	0.00024	0.00044	0.00028	0.00110	0.01170
	ΔP_{tie}	0.00072	0.00241	0.00012	0.0007	0.00260
Undershoot (U_{sh})	ΔF_1	-0.00600	-0.0102	-0.00086	-0.0109	-0.0245
	ΔF_2	-0.00062	-0.0008	-0.00035	-0.0035	-0.0228
	ΔP_{tie}	-0.00803	-0.0087	-0.00564	-0.0022	-0.0044

Table 3. Comparison performance of several algorithms for scenario 2.

power systems and indicates that SGO-FOPIDD2 controllers performs excellent as compared to other controllers having a smaller number of oscillations.

Conclusion and future study

This article introduces the SGO-based FOPIDD2 methodology as an improvement for Load Frequency Control (LFC) problems in various two-area power systems that include solar, wind, hydro, reheat thermal, electric vehicles, and capacitive energy storage. The superiority of the SGO-based FOPIDD2 controller is proven by a comparison assessment employing recent metaheuristic algorithms as well as different control methodologies. The SGO-based FOPIDD2 approach exhibits superior performance compared to GWO based FOPIDD2, JSO based FOPIDD2, and WCA based I-TD controllers in respect of settling times, and peak under/overshoots. The FOPIDD2 controllers improved Ts by 19.78%, 12.87%, and 26.09% when compared to the PIDD2 controller. In the same manner, the SGO algorithms also improved time settling by 13.98%, 47.67%, and 54.54% when compared to the jellyfish search algorithm, while significantly reducing maximum O_{sh} by 87.09%, 81.12%, and 76.78%, and U_{sh} by 81.19%, 66.54%, and 93.76% for (ΔP_{tie}), (ΔF_1), and (ΔF_2). Furthermore, the results reveal that SGO based FOPIDD2 superiorly perform with the integration of capacitive energy storages and electrical vehicles in respect of improved settling time, decrease overshoot and undershoot values as compared to without including the effecting of energy storage unit. The recommended SGO-FOPIDD2 has been found to be resilient and exhibits exceptional performance when faced with different sizes of load disturbances and variations in system components. In future, the proposed work may be further enhanced by incorporating with an additional inertial system and can be employed with some recent and advanced optimization techniques.

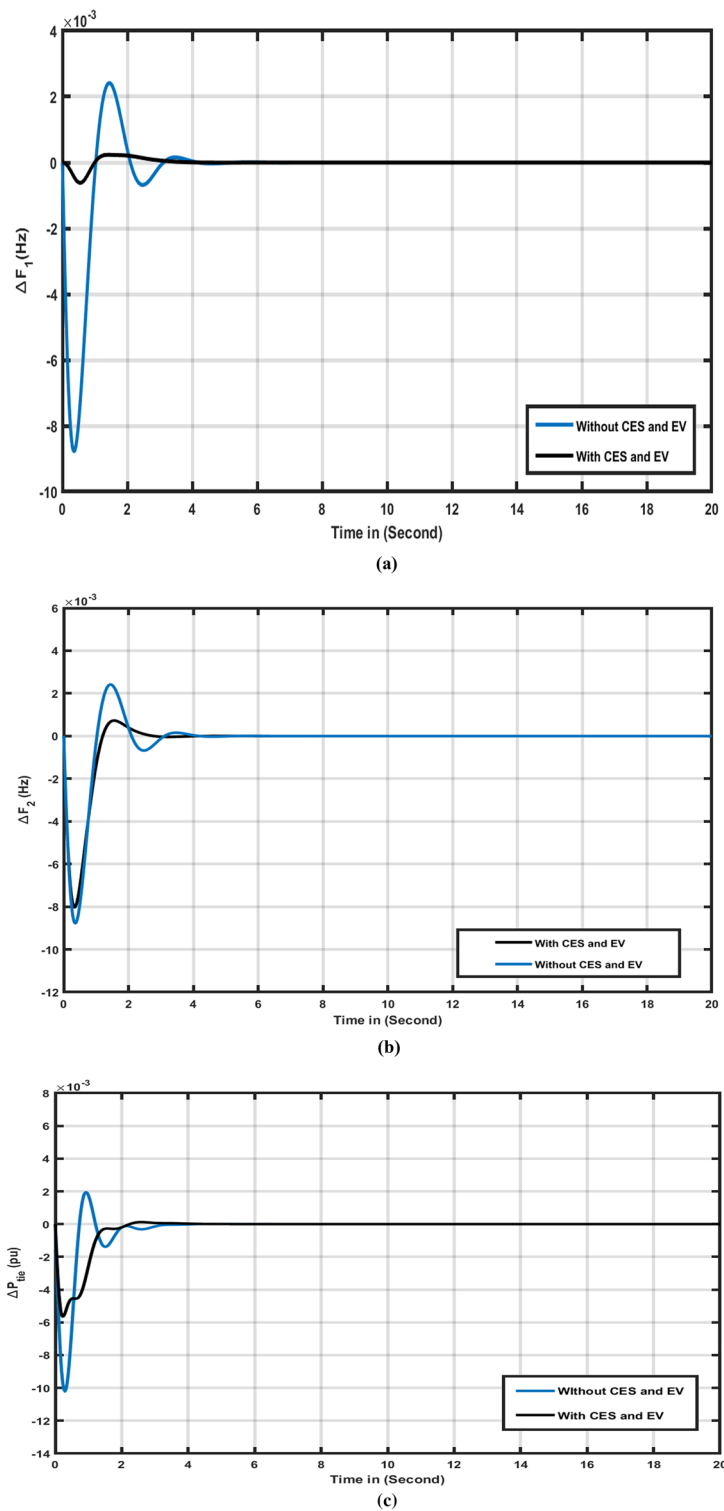


Figure 7. Transient response of HPS with various algorithm techniques in: (a) ΔF_1 (b) ΔF_2 , (c) ΔP_{tie} .

Transient parameters	System consideration	Without CES and EV	With CES and EVS
Time settling (Ts)	ΔF_1	4.00	2.88
	ΔF_2	4.33	2.60
	ΔP_{tie}	3.65	2.51
Overshoot (O_{sh})	ΔF_1	0.0024142	0.0002347
	ΔF_2	0.0024140	0.0007254
	ΔP_{tie}	0.0019389	0.0001220
Undershoot (U_{sh})	ΔF_1	-0.008772	-0.0006158
	ΔF_2	-0.008771	-0.008038
	ΔP_{tie}	-0.0102192	-0.0056199

Table 4. Comparison performance for case 3.

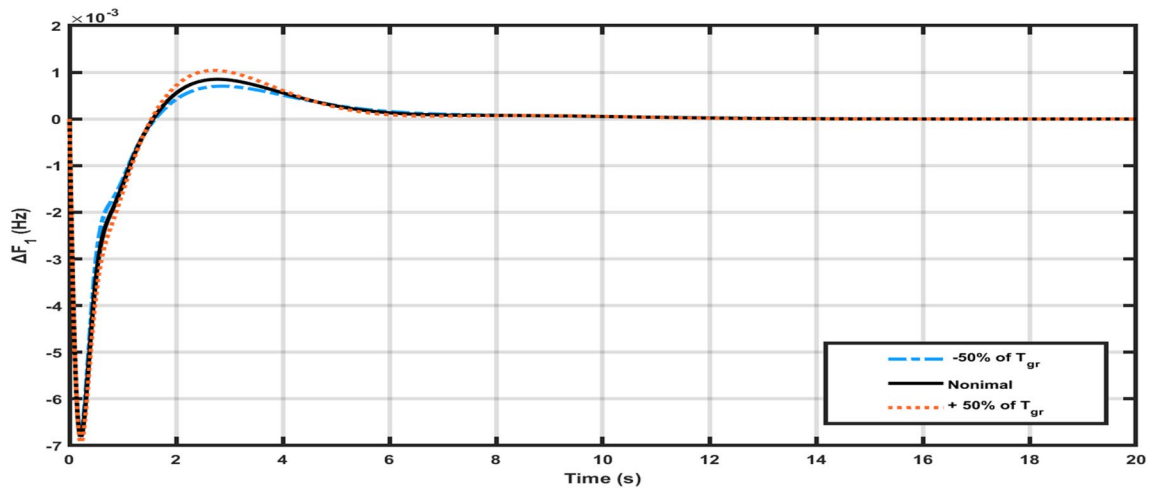


Figure 8. Variation of T_{gr} power system parameters for ΔF_1 .

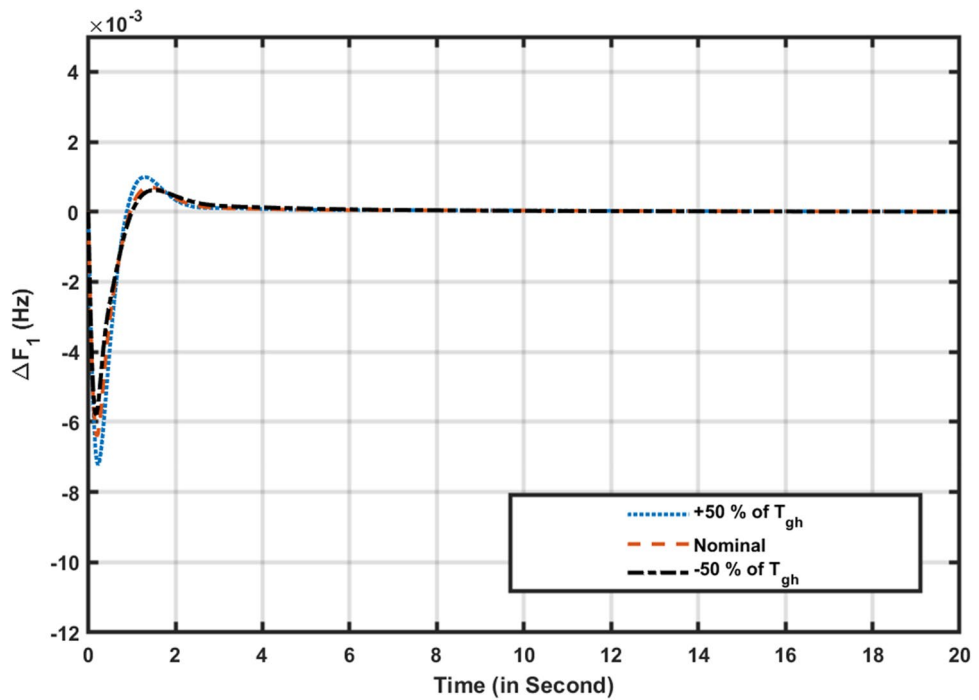


Figure 9. Variation of T_{gh} power system parameters for ΔF_1 .

Transient contents	Parameters of power system	% change	$\Delta F1$	$\Delta F2$	ΔP_{uc}
Overshoot	T_{gr}	+ 50%	0.001040	0.00430	0.000123
		- 50%	0.001060	0.000440	0.000129
		Nominal	0.001020	0.000420	0.000122
	T_{gh}	+ 50%	0.0002201	0.0003407	0.0007254
		- 50%	0.0002226	0.0003467	0.0007294
		Nominal	0.0002105	0.0003458	0.0007798
	K_w	+ 50%	0.0003708	0.0003834	0.0017100
		- 50%	0.0003669	0.0003785	0.0017600
		Nominal	0.0003669	0.0003809	0.0017340
Undershoot	T_{gr}	+ 50%	- 0.006741	- 0.0008692	- 0.006016
		- 50%	- 0.006720	- 0.000884	- 0.006001
		Nominal	- 0.000268	- 0.000351	- 0.000622
	T_{gh}	+ 50%	- 0.000220	- 0.000392	- 0.000583
		- 50%	- 0.000223	- 0.000367	- 0.000603
		Nominal	- 0.000223	- 0.000367	- 0.000603
	K_w	+ 50%	- 0.006016	- 0.005648	- 0.007830
		Nominal	- 0.006080	- 0.005490	- 0.008090
		+ 50%	- 0.006267	- 0.0005878	- 0.008689
Time settling	T_{gr}	+ 50%	6.12	6.85	6.89
		- 50%	6.61	6.93	6.87
		Nominal	6.10	6.80	6.84
	T_{gh}	+ 50%	3.20	3.66	3.66
		- 50%	3.22	3.56	3.62
		Nominal	3.18	3.60	3.60
	K_w	Nominal	4.52	3.64	4.78
		- 50%	4.81	3.63	4.80
		+ 50%	4.88	3.66	4.82

Table 5. Variations in hybrid power system parameters.

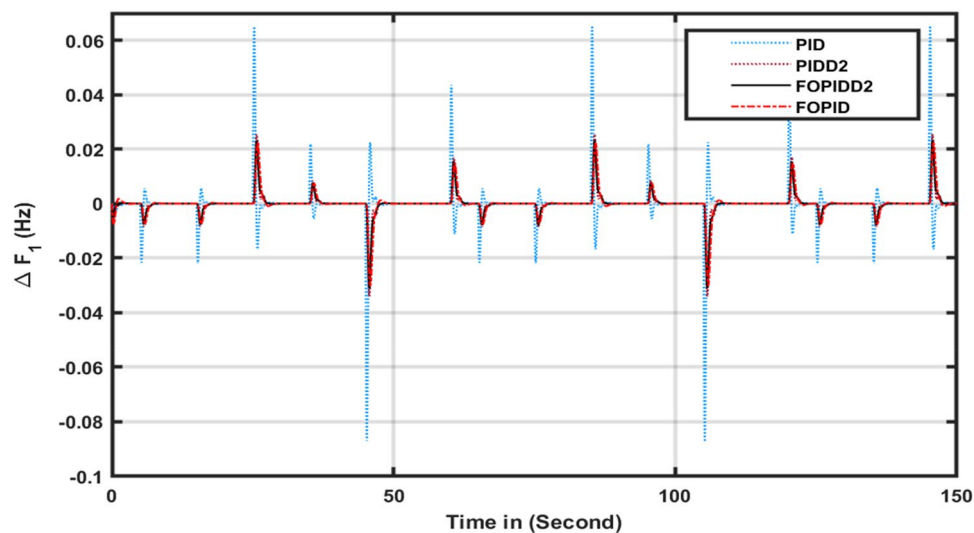


Figure 10. Random load variations for hybrid power systems.

Data availability

All data generated or analyzed during this study are included in this published article [and its supplementary information files].

Received: 29 February 2024; Accepted: 18 April 2024

Published online: 24 April 2024

References

- Ravi, C., Rai, J. N. & Yogendra, A. FOPTID+1 controller with capacitive energy storage for AGC performance enrichment of multi-source electric power systems. *Electr. Power Syst. Res.* **221**, 109450. <https://doi.org/10.1016/j.epsr.2023.109450> (2023).
- Sawle, Y., Gupta, S. C. & Bohre, A. K. Review of hybrid renewable energy systems with comparative analysis of off-grid hybrid system. *Renew. Sustain. Energy Rev.* **81**, 2217–2235 (2018).
- Hassan, A. *et al.* Optimal frequency control of multi-area hybrid power system using new cascaded TID-PIAD μ n controller incorporating electric vehicles. *Fractal Fract.* **6**, 548 (2022).
- Rajendra, K. K., Amit, K. & Sidhartha, P. A modified grey wolf optimization with cuckoo search algorithm for load frequency controller design of hybrid power system. *Appl. Soft Comput.* **124**, 109011. <https://doi.org/10.1016/j.asoc.2022.109011> (2022).
- Alrajhi, H. A novel synchronization method for seamless microgrid transitions. *Arab. J. Sci. Eng.* <https://doi.org/10.1007/s13369-023-08454-9> (2023).
- Khamies, M., Magdy, G., Selim, A. & Kamel, S. An improved Rao algorithm for frequency stability enhancement of nonlinear power system interconnected by AC/DC links with high renewables penetration. *Neural Comput. Appl.* **34**, 2883–2911 (2021).
- Ahmed, E. M., Mohamed, E. A., Elmelegi, A., Aly, M. & Elbaksawi, O. Optimum modified fractional order controller for future electric vehicles and renewable energy-based interconnected power systems. *IEEE Access* **9**, 29993–30010 (2021).
- Magdy, G., Shabib, G., Elbaset, A. A. & Mitani, Y. Optimized coordinated control of LFC and SMES to enhance frequency stability of a real multi-source power system considering high renewable energy penetration. *Prot. Control. Mod. Power Syst.* **3**, 39 (2018).
- Khamies, M., Magdy, G., Kamel, S. & Khan, B. Optimal model predictive and linear quadratic gaussian control for frequency stability of power systems considering wind energy. *IEEE Access* **9**, 116453–116474 (2021).
- Benazeer, B. *et al.* Application of an intelligent fuzzy logic based sliding mode controller for frequency stability analysis in a deregulated power system using OPAL-RT platform. *Energy Rep.* **11**, 510–534. <https://doi.org/10.1016/j.egy.2023.12.023> (2024).
- Ngyuen, G. N., Jagatheesan, K., Ashour, A. S., Anand, B. & Dey, N. Ant colony optimization based load frequency control of multi-area interconnected thermal power system with governor dead-band nonlinearity. In *Smart trends in systems, security and sustainability* 157–167 (Springer, 2018).
- Jagatheesan, K., Anand, B., Dey, N., Ashour, A. S. & Balas, V. E. Load frequency control of hydro-hydro system with fuzzy logic controller considering non-linearity. In *Recent developments and the new direction in soft-computing foundations and applications* 307–318 (Springer, 2018).
- Dritsas, L. *et al.* Modelling issues and aggressive robust load frequency control of interconnected electric power systems. *Int. J. Control* **95**, 753–767 (2022).
- Qi, X., Zheng, J. & Mei, F. Model predictive control-based load frequency regulation of grid-forming inverter-based power systems. *Front. Energy Res.* **10**, 932788. <https://doi.org/10.3389/fenrg.2022.932788> (2022).
- Jagatheesan, K., Baskaran, A., Dey, N., Ashour, A. S. & Balas, V. E. Load frequency control of multi-area interconnected thermal power system: Artificial intelligence-based approach. *Int. J. Autom. Control* **12**, 126–152 (2018).
- Ly, X., Sun, Y., Wang, Y. & Dinavahi, V. Adaptive event-triggered load frequency control of multi-area power systems under networked environment via sliding mode control. *IEEE Access* **8**, 86585–86594 (2020).
- Eltamaly, A. M., Zaki Diab, A. A. & Abo-Khalil, A. G. Robust control based on H_{∞} and linear quadratic Gaussian of load frequency control of power systems integrated with wind energy system. In *Control and operation of grid-connected wind energy systems* 73–86 (Springer, 2021).
- Yu, X. & Tomsovic, K. Application of linear matrix inequalities for load frequency control with communication delays. *IEEE Trans. Power Syst.* **19**, 1508–1515 (2004).
- Bu, X., Yu, W., Cui, L., Hou, Z. & Chen, Z. Event-triggered data-driven load frequency control for multiarea power systems. *IEEE Trans. Ind. Inform.* **18**, 5982–5991 (2022).
- Yakout, A. H., Koth, H., Hasanien, H. M. & Aboras, K. M. Optimal fuzzy PIDF load frequency controller for hybrid microgrid system using marine predator algorithm. *IEEE Access* **9**, 54220–54232 (2021).
- Kerdphol, T., Rahman, F. S., Mitani, Y., Watanabe, M. & Kufeoglu, S. Robust virtual inertia control of an Islanded microgrid considering high penetration of renewable energy. *IEEE Access* **6**, 625–636 (2018).
- Habib, D. Optimal control of PID-FUZZY based on gravitational search algorithm for load frequency Control. *Int. J. Eng. Res.* **8**, 50013–50022 (2019).
- Daraz, A., Malik, S. A., Basit, A., Aslam, S. & Zhang, G. Modified FOPID controller for frequency regulation of a hybrid interconnected system of conventional and renewable energy sources. *Fractal Fract.* **7**, 89 (2023).
- Arya, Y. A novel CFFOPI-FOPID controller for AGC performance enhancement of single and multi-area electric power systems. *ISA Trans.* **100**, 126–135 (2020).
- Zhang, G. *et al.* Driver training based optimized fractional order PI-PDF controller for frequency stabilization of diverse hybrid power system. *Fractal Fract.* **7**, 315. <https://doi.org/10.3390/fractalfract7040315> (2023).
- Arya, Y. AGC performance enrichment of multi-source hydrothermal gas power systems using new optimized FOPPID controller and redox flow batteries. *Energy* **127**, 704–715 (2017).
- Ali, M., Koth, H., Aboras, K. M. & Abbasy, N. H. Design of cascaded PI-fractional order PID controller for improving the frequency response of hybrid microgrid system using gorilla troops optimizer. *IEEE Access* **9**, 150715–150732 (2021).
- Arya, Y. AGC of PV-thermal and hydro-thermal power systems using CES and a new multi-stage FPIDF-(1+PI) controller. *Renew. Energy* **134**, 796–806 (2019).
- Elkasem, A. H. A., Khamies, M., Hassan, M. H., Agwa, A. M. & Kamel, S. Optimal design of TD-TI controller for LFC considering renewables penetration by an improved chaos game optimizer. *Fractal Fract.* **6**, 220 (2022).
- Mohamed, T. H., Shabib, G., Abdelhameed, E. H., Khamies, M. & Qudaih, Y. Load frequency control in single area system using model predictive control and linear quadratic gaussian techniques. *Int. J. Electr. Energy* **3**, 141–143 (2015).
- Raju, M., Saikia, L. & Sinha, N. Automatic generation control of a multi-area system using ant lion optimizer algorithm based PID plus second order derivative controller. *Int. J. Electr. Power Energy Syst.* **80**, 52–63 (2016).
- Kumari, S., Shankar, G. & Das, B. Integral-tilt-derivative controller based performance evaluation of load frequency control of deregulated power system. In *Modeling, simulation and optimization* 189–200 (Springer, 2021).
- Daraz, A. *et al.* Optimized fractional order integral-tilt derivative controller for frequency regulation of interconnected diverse renewable energy resources. *IEEE Access* **10**, 43514–43527. <https://doi.org/10.1109/ACCESS.2022.3167811> (2022).
- Ahmed, M., Magdy, G., Khamies, M. & Kamel, S. Modified TID controller for load frequency control of a two-area interconnected diverse-unit power system. *Int. J. Electr. Power Energy Syst.* **135**, 107528 (2022).
- Hasan, N., Asaidan, I., Sajid, M., Khatoun, S. & Farooq, S. Robust self tuned AGC controller for wind energy penetrated power system. *Ain Shams Eng. J.* **13**(4), 101663 (2022).
- Singh, B., Slowik, A. & Bishnoi, S. K. A dual-stage controller for frequency regulation in a two-area realistic diverse hybrid power system using bull-lion optimization. *Energies* **15**, 8063. <https://doi.org/10.3390/en15218063> (2022).
- Rout, U. K., Sahu, R. K. & Panda, S. Design and analysis of differential evolution algorithm based automatic generation control for interconnected power system. *Ain Shams Eng. J.* **4**, 409–421 (2012).
- Barkat, M. Novel chaos game optimization tuned-fractional-order PID fractional-order PI controller for frequency control of interconnected power systems. *Prot. Contr. Modern Power Syst.* **7**, 16 (2022).

39. Guha, D., Roy, P. K. & Banerjee, S. Krill herd algorithm for automatic generation control with flexible AC transmission system controller including superconducting magnetic energy storage units. *J. Eng.* **2016**, 147–161 (2016).
40. Daraz, A. *et al.* Improved-fitness dependent optimizer based FOI-PD controller for automatic generation control of multi-source interconnected power system in deregulated environment. *IEEE Access* **8**, 197757–197775 (2020).
41. Mishra, S. *et al.* Modified multiverse optimizer technique-based two degree of freedom fuzzy PID controller for frequency control of microgrid systems with hydrogen aqua electrolyzer fuel cell unit. *Neural Comput. Appl.* **34**, 18805–18821. <https://doi.org/10.1007/s00521-022-07453-5> (2022).
42. Nayak, P. C., Nayak, B. P., Prusty, R. C. & Panda, S. Sunflower optimization based fractional order fuzzy PID controller for frequency regulation of solar-wind integrated power system with hydrogen aqua equalizer fuel cell unit. *Energy Sources, Part A Recovery, Util., Environ. Effects* <https://doi.org/10.1080/15567036.2021.1953636> (2021).
43. Priyadarshani, S., Subhashini, K. R. & Satapathy, J. K. Pathfinder algorithm optimized fractional order tilt-integral-derivative (FOTID) controller for automatic generation control of multi-source power system. *Microsyst. Technol.* **27**, 23–35 (2021).
44. Sahu, R. K., Sekhar, G. C. & Priyadarshani, S. Differential evolution algorithm tuned tilt integral derivative controller with filter controller for automatic generation control. *Evol. Intell.* **14**(1), 5–20 (2021).
45. Kumari, S. & Shankar, G. Novel application of integral-tilt-derivative controller for performance evaluation of load frequency control of interconnected power system. *IET Gener. Transm. Distrib.* **12**(14), 3550–3560 (2018).
46. Azizi, M. *et al.* Squid game optimizer (SGO): A novel metaheuristic algorithm. *Sci. Rep.* **13**, 5373. <https://doi.org/10.1038/s41598-023-32465-z> (2023).
47. Mohamed, E. A. *et al.* An optimized hybrid fractional order controller for frequency regulation in multi-area power systems. *IEEE Access* **8**, 213899–213915 (2020).
48. Ali, T. *et al.* Load frequency control and automatic voltage regulation in four-area interconnected power systems using a gradient-based optimizer. *Energies* **16**, 2086. <https://doi.org/10.3390/en16052086> (2023).
49. Arya, Y., Ahmad, R., Nasiruddin, I. & Ahmer, M. F. LFC performance advancement of two-area RES penetrated multi-source power system utilizing CES and a new CFOTID controller. *J. Energy Storage* **87**, 111366. <https://doi.org/10.1016/j.est.2024.111366> (2024).
50. Singh, K., Dahiya, M., Grover, A., Adlakha, R. & Amir, M. An effective cascade control strategy for frequency regulation of renewable energy-based hybrid power system with energy storage system. *J. Energy Storage* **68**, 107804 (2023).
51. Dhundhara, S. & Verma, Y. P. Capacitive energy storage with optimized controller for frequency regulation in realistic multisource deregulated power system. *Energy* **147**, 1108–1128 (2018).
52. Falahati, S., Taher, S. A. & Shahidehpour, M. Grid secondary frequency control by optimized fuzzy control of electric vehicles. *IEEE Trans. Smart Grid* **9**, 5613–5621 (2018).
53. Luo, X., Xia, S. & Chan, K. W. Adcentralized charging control strategy for plug-in electric vehicles to mitigate wind farm intermittency and enhance frequency regulation. *J. Power Sources* **248**, 604–614 (2014).
54. Ahmed, E. M. *et al.* Modified frequency regulator based on TP^A-TD^{FF} controller for interconnected microgrids with incorporating hybrid renewable energy sources. *Mathematics* **11**, 28. <https://doi.org/10.3390/math11010028> (2023).
55. Kumar, D., Mathur, H. D., Bhanot, S. & Bansal, R. C. Frequency regulation in islanded microgrid considering stochastic model of wind and PV. *Int. Trans. Electr. Energy Syst.* **29**, e12049. <https://doi.org/10.1002/2050-7038.12049> (2019).
56. Khokhar, B., Dahiya, S. & Parmar, K. P. S. A robust cascade controller for load frequency control of a standalone microgrid incorporating electric vehicles. *Electr. Power Compon. Syst.* **48**, 711–726 (2020).
57. Ray, P. K., Mohanty, S. R. & Kishor, N. Proportional–integral controller based small-signal analysis of hybrid distributed generation systems. *Energy Convers. Manag.* **52**, 1943–1954 (2011).
58. Das, D. C., Roy, A. & Sinha, N. GA based frequency controller for solar thermal–diesel–wind hybrid energy generation/energy storage system. *Int. J. Electr. Power Energy Syst.* **43**(262–279), 64 (2012).
59. Khudhair, M., Ragab, M., AboRas, K. M. & Abbasy, N. H. Robust control of frequency variations for a multi-area power system in smart grid using a newly wild horse optimized combination of PID2 and PD controllers. *Sustainability* **14**, 8223. <https://doi.org/10.3390/su14138223> (2022).
60. Izci, D. *et al.* Achieving improved stability for automatic voltage regulation with fractional-order PID plus double-derivative controller and mountain gazelle optimizer. *Int. J. Dynam. Control* <https://doi.org/10.1007/s40435-023-01381-5> (2024).
61. Tabak, A. A novel fractional order PID plus derivative (PIADμDμ2) controller for AVR system using equilibrium optimizer. *COMPEL Int. J. Comput. Math. Electr. Electron. Eng.* **40**(3), 722–743. <https://doi.org/10.1108/COMPEL-02-2021-0044> (2021).

Author contributions

Conceptualization, H.A. and A.A. Data curation, I.K. Formal analysis, I.K. Methodology, A.D. and A.B. Software, A.D. and A.A.; Supervision, H.A.; Validation, H.A., A.B., A.A., A.A. and I.K.; Writing—original draft, A.D.; Writing—review & editing, H.A., A.B., A.A., A.A. and I.K.

Competing interests

The authors declare no competing interests.

Additional information

Supplementary Information The online version contains supplementary material available at <https://doi.org/10.1038/s41598-024-60028-3>.

Correspondence and requests for materials should be addressed to A.D. or A.R.A.

Reprints and permissions information is available at www.nature.com/reprints.

Publisher's note Springer Nature remains neutral with regard to jurisdictional claims in published maps and institutional affiliations.



Open Access This article is licensed under a Creative Commons Attribution 4.0 International License, which permits use, sharing, adaptation, distribution and reproduction in any medium or format, as long as you give appropriate credit to the original author(s) and the source, provide a link to the Creative Commons licence, and indicate if changes were made. The images or other third party material in this article are included in the article's Creative Commons licence, unless indicated otherwise in a credit line to the material. If material is not included in the article's Creative Commons licence and your intended use is not permitted by statutory regulation or exceeds the permitted use, you will need to obtain permission directly from the copyright holder. To view a copy of this licence, visit <http://creativecommons.org/licenses/by/4.0/>.

© The Author(s) 2024